

Digital Ripple Correlation Control for Photovoltaic Applications

Jonathan W. Kimball, *Senior Member*

SmartSpark Energy Systems, Inc.
60 Hazelwood Dr.
Champaign, IL 61820

Philip T. Krein, *Fellow*

Grainger Center for Electric Machinery and Electromechanics
University of Illinois at Urbana-Champaign
1406 W. Green St.
Urbana, IL 61801

Abstract – Ripple correlation control (RCC) is a fast, robust online optimization technique. RCC is particularly suited for switching power converters, where the inherent ripple provides information about the system operating point. The present work examines a digital formulation that has reduced power consumption and greater robustness. A maximum power point tracker for a photovoltaic panel demonstrates greater than 99% tracking accuracy and fast convergence.

Keywords – ripple correlation control, optimal control, maximum power point tracking, photovoltaic

I. INTRODUCTION

Maximum power point trackers (MPPT) are frequently used to extract maximum power from a photovoltaic panel. Many methods have been studied over the past three decades [1]. Ripple correlation control (RCC) was introduced as a dynamic optimization technique that can be used as the basis for a MPPT or for motor efficiency maximization [2-16]. RCC uses ripple that exists in all switching power converters to extract information about the operating point. Parameter sensitivity is minimized since the signals involved reflect energy dynamics. Convergence is inherently fast, up to the time scale of a few switching periods.

Many modern MPPT techniques, and related online optimization techniques, are implemented digitally. In some cases, such as incremental conductance methods [17], digital implementation is fundamental. In others, such as fractional open-circuit voltage (fractional V_{oc}) [18], an analog system is possible but a digital controller is far superior. Digital controllers are easily reconfigurable and support a broad range of time scales. In many cases, a microprocessor consumes less power than an equivalent analog circuit.

In the present work, RCC is adapted to the digital domain. Previous work has been formulated for continuous-time signals. In principle, all of the relevant signals could be sampled quickly (with respect to Nyquist sampling criteria) to reconstruct the previously reported control law. However, since many of the characteristics of the signals are known, a

This work was supported in part by the National Science Foundation under NSF Award ECS 06-21643. Both authors are affiliated with both the Grainger CEME at the University of Illinois and with SmartSpark Energy Systems, Inc.

simpler approach is possible. Discrete-time RCC (DRCC) reduces the previous complex algorithm to a sample timing problem: sample the correct signals at the correct times, and the same results are achieved as in analog RCC.

First, this paper will present the background of RCC to frame the problem. Next, the DRCC control law will be derived. Since the objective is to optimize an energy function, energy storage elements complicate implementation. A method for mitigating the effect of solar panel capacitance will be shown for an MPPT. Finally, experimental results demonstrate tracking effectiveness exceeding 99%.

II. RCC BASIC THEORY

A basic understanding of RCC is fundamental to implementing a digital version. Consider a switching power converter with some state variable z (such as a voltage or current) that affects some cost function J . The objective is to operate the converter such that J is at a maximum or minimum, depending on the application. For an MPPT application, a suitable cost function is $J = P_{panel}$, the power coming from the solar panel, and the state variables could be the panel voltage, current, or both. An extremum of J is located where $\frac{dJ}{dz} = 0$ if J is only a function of z . An effective method for driving a function to zero is integral control, where the input u to the plant is determined by

$$u = k \int \frac{dJ}{dz} dt \quad (1)$$

However, this sort of derivative (dJ/dz) is generally unavailable. Multiplying the integrand by a positive function affects the convergence rate but not the operating point. A good choice is $\left(\frac{dz}{dt}\right)^2$, which is positive except at isolated points as long as the converter is switching. Multiplying this into the integrand of (1) gives a new control law that simplifies by the chain rule as

$$u = k \int \frac{dJ}{dz} \frac{dz}{dt} \frac{dz}{dt} dt = k \int \frac{dJ}{dt} \frac{dz}{dt} dt = k \int J \dot{z} dt. \quad (2)$$

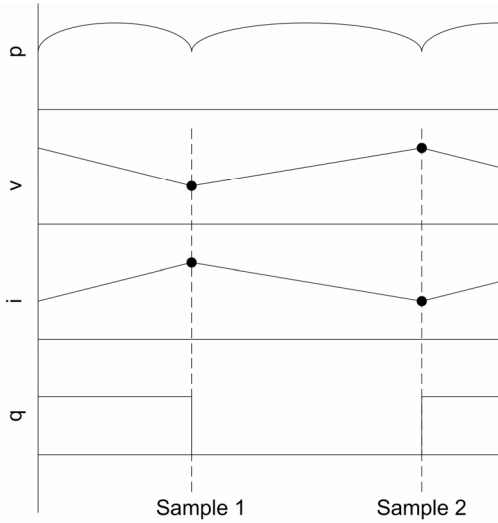


Fig. 1. Sample timing related to switching function q , panel voltage v , current i , and power p .

Time derivatives are readily obtained with analog circuits. Previous experimental MPPTs used an analog multiplier to generate the P_{panel} waveform, then another analog multiplier to generate $\dot{P}_{panel} \dot{V}_{panel}$. The integral of that output determined the duty cycle of a boost converter. The result was a fast and effective MPPT process [4][16].

Simplifications of (2) have been proposed. For example, a filter that preserves phase information over a limited frequency range can be used in place of a derivative. Often, $\text{sgn}(\dot{z})$ is related, directly or indirectly, to the switching function, and the sign of the derivative is adequate for the control process. In such a case, the multiplication $\dot{J} \times \text{sgn}(\dot{z})$ can be replaced with a synchronous demodulator. Still, computing J itself often involves a multiplication, which can be inconvenient in an analog circuit. Analog multipliers are available, but are relatively expensive and power-hungry. For example, an Analog Devices AD633 consumes 4 mA at ± 15 V, or 120 mW.

III. DIGITAL RCC

Digital multiplication is straightforward. Microcontrollers with hardware multipliers are available at a number of price points and include low-power device families like the Texas Instruments MSP430 family. An obvious implementation is to sample analog signals at a high rate and implement a direct discrete-time version of (2). However, this offers no special advantages compared to an all-analog process.

An alternative form results from a more thorough study of the RCC principles. Suppose, as is often the case, that z is piecewise linear in time, so \dot{z} is piecewise constant, i.e.,

$$\dot{z} = \begin{cases} w_+ & \text{mod}(t, T) \in [0, DT) \\ w_- & \text{mod}(t, T) \in [DT, T) \end{cases} \quad (3)$$

Here, w_+ and w_- are the positive and negative slopes of a triangular ripple signal. D is the duty cycle and T is the period, neither of which need be constant. This form of the derivative leads to direct computation of (2),

$$\begin{aligned} u(T) &= u(0) + kw_+ \int_0^{DT} \dot{J} dt + kw_- \int_{DT}^T \dot{J} dt \\ u(T) &= u(0) + kw_+ (J(DT) - J(0)) \\ &\quad + kw_- (J(T) - J(DT)) \end{aligned} \quad (4)$$

In periodic steady state, the cost function is also periodic, and

$$\begin{aligned} J(0) &= J(T) \\ w_+ D + w_- (1 - D) &= 0 \end{aligned} \quad (5)$$

When eq. (5) is used in (4), the result is a greatly reduced control law:

$$u(T) = u(0) + \frac{kw_+}{1-D} (J(DT) - J(0)) \quad (6)$$

The plant input in a subsequent cycle is a function of its prior value and of the cost function sampled at only two points in time. A key implication of (6) is the form of $J(t)$: at the optimum operating condition, not only will $J(t)$ be periodic, but in addition its value at the switching time $J(DT)$ will match the value at the beginning and end of the cycle. This symmetry is shown in Fig. 1, in which a converter has reached the maximum power point in a solar application. In this condition, the operation sweeps through the instantaneous maximum point during each sub-cycle, and the output is as close to the actual maximum power point as possible, given ripple. For an arbitrary non-optimum operating point, one would expect power to increase during one portion of the cycle

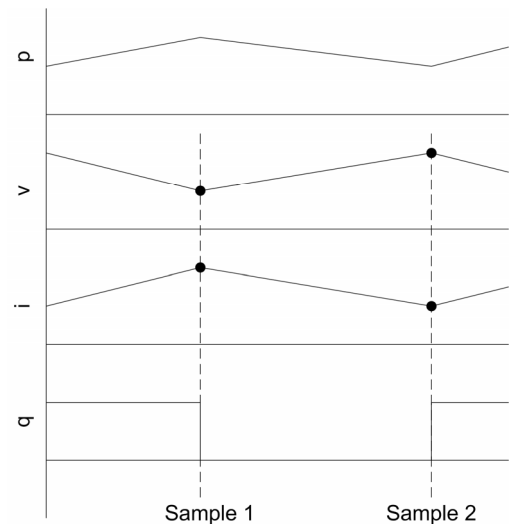


Fig. 2. Sample timing related to switching function q , panel voltage v , current i , and power p . System operating point is not at the maximum power point (voltage is too high).

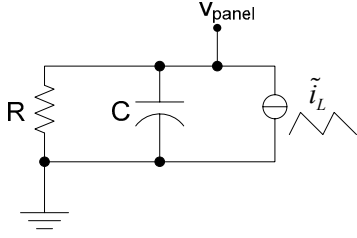


Fig. 3. Small-signal equivalent circuit.

and decrease during the other, such as the operating point shown in Fig. 2. If the maximum occurs midway through the conduction period, then the converter can be said to be operating at maximum power.

Further simplifications can be made. For example, the controller could act on the sign of the difference in J , rather than the value, which can be categorized as delta modulation [19]. The typical control implementation is:

1. Sample voltages and currents at $t = 0$ and at $t = DT$ as shown in Fig. 1.
2. Compute $J(0)$ and $J(DT)$, in this case values of power.
3. Update the converter duty cycle based on the sign of $(J(DT) - J(0))$.

The resulting controller inherits most benefits of analog RCC and gains benefits from digital implementation. For example, RCC requires ripple to gain information about the operating point, a requirement similar to persistence of excitation. In a digital implementation, mode switching can be used to ensure adequate ripple and adequate signal-to-noise ratio (SNR). Protection modes and user interface also become easier to implement.

The control method derived resembles perturb-and-observe (P&O) methods [20], but in fact provides a number of distinctions. One key difference is the time scale. In P&O, a perturbation is added to the operating point and steady-state characteristics are compared. In DRCC, two specific points in the limit cycle of the switching converter are compared. DRCC is fundamentally faster than P&O since the plant need not reach steady-state between updates. A second difference is the action. A DRCC approach fundamentally moves the dynamic operation to an optimum point, rather than sequentially adjusting duty ratio, then checking the result. A converter operated with DRCC does not display duty ratio variation in steady state. Rather, it converges to a fixed operating point coinciding with maximum power from the panel. Stability of analog RCC is well established [12].

IV. PHOTOVOLTAIC MPPT: STORED ENERGY EFFECTS

RCC has been previously demonstrated for solar applications. The study in [16] used a boost converter. The ideal choice of variables is [16]

$$\begin{aligned} J &= P_{panel} = v_{panel} i_{panel} \\ z &= v_{panel} \\ u &= D \end{aligned} \quad (7)$$

This choice of z reduces the impact of solar cell capacitance, but complicates the timing for a digital implementation. If $z = i_{panel}$, then $\text{sgn}(\dot{z}) = (2q - 1)$, where q is the switching function. Using panel voltage instead results in a phase shift between q and $\text{sgn}(\dot{z})$.

All solar panels have capacitance that results from stored charge at the cell p-n junctions. This capacitance and the incremental resistance of the panel lead to a phase shift between the imposed current ripple and the resulting voltage ripple. A small-signal equivalent circuit is shown in Fig. 3. The incremental resistance is dominated by a term that decays exponentially with terminal voltage. The capacitance grows exponentially with terminal voltage. So the time constant, which governs the phase shift, is nearly constant at about 17 μs over a broad operating range.

Fig. 4 shows current and voltage waveforms with capacitance. The correct sampling times can be found from a solution of the differential equations that govern the circuit of

Fig. 3. The sample time is when $\frac{dv_{panel}}{dt}(t_{sample}) = 0$, or

$$t_{sample} = DT + RC \ln \left(\frac{1 - \exp\left(\frac{(1-D)T}{RC}\right)}{(1-D)\left(1 - \exp\left(\frac{T}{RC}\right)\right)} \right) \quad (8)$$

The computation implied by (8) is too complicated for a low-cost microcontroller. However, a plot of the sample time versus duty cycle, shown in Fig. 5, indicates that a quadratic or piecewise linear approximation is appropriate. Either

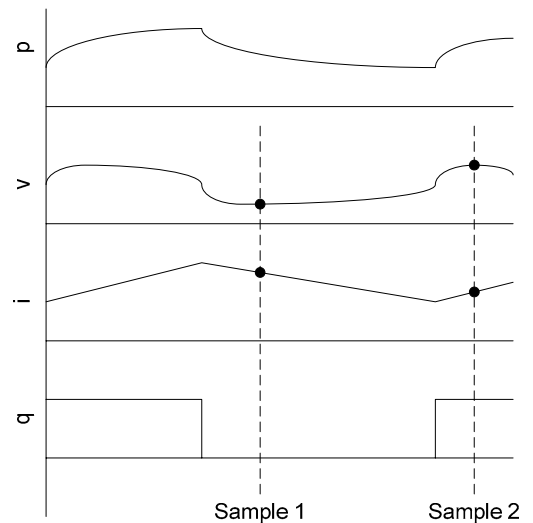


Fig. 4. Timing with $z = v_{panel}$.

approximation fits the actual curve within 2% and is easily implemented in a microcontroller. The piecewise linear approach was used in the experimental results reported here.

V. EXPERIMENTAL MPPT

An experimental digital MPPT was built to demonstrate the effectiveness of DRCC. The panel was a Solec S-5136. A boost converter was built with a 3.4 mH inductor, an IRF3710 MOSFET, and a MBR1545CT Schottky diode. Switching frequency was set at 25 kHz, for a compromise between manageable component sizes and detectable ripple.

An MSP430F148 was used to implement the algorithm. This microcontroller has a hardware 8x8 multiplier and a 12-bit ADC. Typical power consumption is 1.2 mA at 3 V (including peripherals), or 3.6 mW. To improve signal integrity, both voltage and current signals were split into dc and ac components. The ac components were sampled by means of 74HC4066 analog switches at the times shown in Fig. 4. Current was sensed with a LEM LA55-P Hall effect current sensor with five primary turns.

A mode-switching algorithm was used to improve robustness and overall performance. First, the converter is turned off briefly to sample the open-circuit voltage V_{oc} and to null offsets in the analog signal path. Next, a constant voltage fraction algorithm [18] is used to establish an initial condition. This puts the panel near its maximum power point, a regime where ripple is adequate for detection in the DRCC approach. Then, the DRCC algorithm is enabled to drive the panel to the precise maximum power point. The currents and voltages are only sampled every 20th PWM cycle to reduce computational burdens. The sample rate can be increased up to the PWM frequency for fast convergence.

Fig. 6 shows panel current and voltage. At $t = 0$, the converter is disabled and the panel is at open circuit. Then, the constant voltage fraction (CVF) algorithm begins to operate.

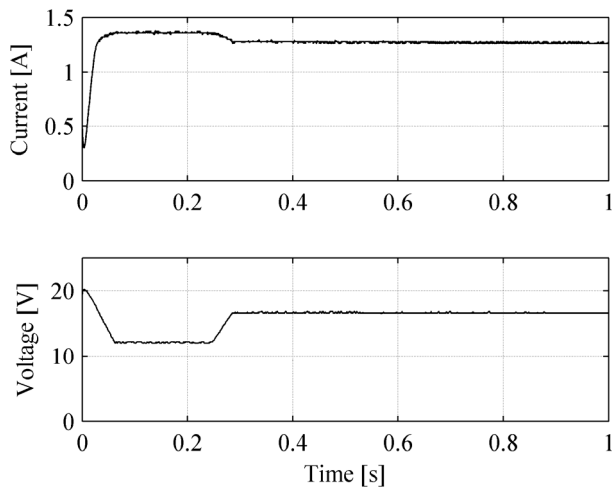


Fig. 6. Panel current and voltage through mode-switching algorithm. At $t = 0$, the system is in the open-circuit mode.

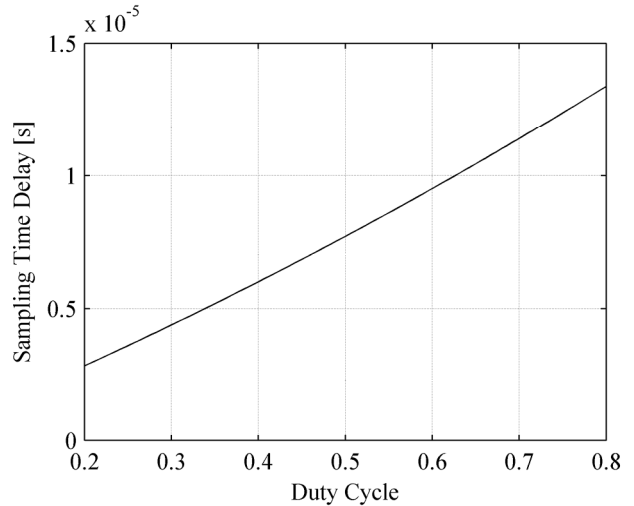


Fig. 5. Variation of sampling delay t_{sample} with duty cycle for experimental solar panel.

The fraction was intentionally set too low (to 0.625). This ensures that the panel will sweep through the maximum power point and arrive at a point where there is adequate voltage ripple. After about 230 ms, the DRCC algorithm is enabled. The panel voltage converges to about 0.824 V_{oc} , which is consistent with manufacturer data.

Fig. 7 shows panel power, computed from the current and voltage waveforms. Again, at $t = 0$, the panel is at open-circuit and the CVF algorithm has just been enabled. The power increases to a maximum of 21.6 W. The transient is slow relative to the panel time constant of 17 μ s, so the peak is equal to steady-state maximum power. The voltage fraction is set too low, so the power drops off. When the DRCC algorithm is enabled, power rises quickly to 21.4 W, or 99.1% of the true maximum. The residual error reflects a small residual error between the assigned panel time constant and the actual value. The actual output is within the designed

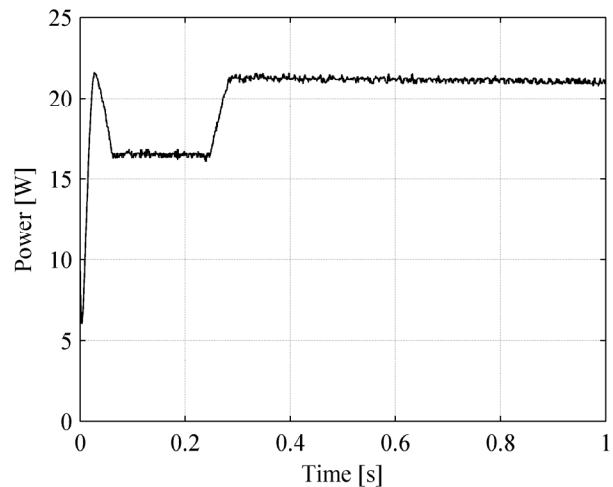


Fig. 7. Panel power corresponding to Fig. 6.

converter ripple band relative to the actual maximum output power. The convergence rates shown in Figs. 6 and 7 represent a convenient setting to illustrate the operation. Convergence can be attained within about five switching cycles if samples are taken during each sub-cycle.

V. CONCLUSIONS

A digital version of RCC has been derived and verified experimentally. With the new DRCC algorithm, greater than 99% tracking effectiveness has been observed for a simple photovoltaic MPPT application. The algorithm can be easily implemented in a low-cost, low-power microcontroller. This expands the range of applications that can use MPPTs. In contrast with widely used perturb and observe techniques, the approach does not vary the duty ratio in a dynamic manner to achieve its results, and the final convergence is within the converter ripple band of the actual maximum power.

DRCC is more general than just photovoltaic applications. The concept and method can be applied to any power maximization or minimization problem in a switching converter application. In particular, DRCC has promise for electric machine efficiency maximization.

REFERENCES

- [1] T. Eswam and P. L. Chapman, "Comparison of photovoltaic array maximum power point tracking techniques," *IEEE Transactions on Energy Conversion*, in press.
- [2] P. Midya, "Nonlinear control and operation of dc to dc switching power converters," Ph.D. dissertation, University of Illinois at Urbana-Champaign, Urbana, IL, 1995.
- [3] P. Midya, P. T. Krein, and R. J. Turnbull, "Self-excited power minimizer/maximizer for switching power converters and switching motor drive applications," U.S. Patent 5,801,519, Sept. 1998.
- [4] P. Midya, P. T. Krein, R. J. Turnbull, R. Reppa, and J. W. Kimball, "Dynamic maximum power point tracker for photovoltaic applications," in *Proc. Power Electronics Specialists Conference*, 1996, pp. 1710-1716.
- [5] R. S. Balog and P. T. Krein, "Automatic tuning of coupled inductor filters," in *Proc. Power Electronics Specialists Conference*, 2002, pp. 591-596.
- [6] N. D. Benavides, T. Eswam, and P. L. Chapman, "Ripple correlation control of a multiple-input dc-dc converter," in *Proc. Power Electronics Specialists Conference*, 2005, pp. 160-164.
- [7] D. Casadei, G. Grandi, and C. Rossi, "Single-phase single-stage photovoltaic generation system based on a ripple correlation control maximum power point tracking," *IEEE Transactions on Energy Conversion*, vol. 21, pp. 562-568, June 2006.
- [8] J. W. Kimball and P. T. Krein, "Continuous-time optimization of gate timing for synchronous rectification," in *Proc. Midwest Symposium on Circuits and Systems*, 1996, pp. 1015-1018.
- [9] P. T. Krein, "Ripple correlation control, with some applications," in *Proc. IEEE International Symposium on Circuits and Systems*, 1999, pp. 283-286.
- [10] Y. H. Lim and D. C. Hamill, "Synthesis, simulation and experimental verification of a maximum power point tracker from nonlinear dynamics," in *Proc. Power Electronics Specialists Conference*, 2001, pp. 199-204.
- [11] D. L. Logue and P. T. Krein, "Observer-based techniques in ripple correlation control applied to power electronic systems," in *Proc. Power Electronics Specialists Conference*, 2001, pp. 2014-2018.
- [12] D. L. Logue and P. T. Krein, "Optimization of power electronic systems using ripple correlation control: a dynamic programming approach," in *Proc. Power Electronics Specialists Conference*, 2001, pp. 459-464.
- [13] D. L. Logue and P. T. Krein, "Machine efficiency optimization using ripple correlation control," in *Proc. Applied Power Electronics Conference*, 2001, pp. 642-648.
- [14] J. R. Wells, P. L. Chapman, and P. T. Krein, "Applications of ripple correlation control of electric machinery," in *Proc. IEEE International Electric Machines and Drives Conference*, 2003, pp. 1498-1503.
- [15] J. R. Wells, P. L. Chapman, and P. T. Krein, "Fundamental aspects of ripple correlation control of electric machinery," in *Proc. Power Electronics Specialists Conference*, 2003, pp. 1659-1662.
- [16] T. Eswam, J. W. Kimball, P. T. Krein, P. L. Chapman, and P. Midya, "Dynamic maximum power point tracking of photovoltaic arrays using ripple correlation control," *IEEE Transactions on Power Electronics*, vol. 21, pp. 1282-1291, Sept. 2006.
- [17] A. F. Boehringer, "Self-adapting dc converter for solar spacecraft power supply," *IEEE Transactions on Aerospace and Electronic Systems*, vol. AES-4, pp. 102-111, Jan. 1968.
- [18] J. J. Schoeman and J. D. v. Wyk, "A simplified maximal power controller for terrestrial photovoltaic panel arrays," in *Proc. Power Electronics Specialists Conference*, 1982, pp. 361-367.
- [19] R. E. Steele, *Delta Modulation*. New York: Wiley, 1975.
- [20] O. Wasynczuk, "Dynamic behavior of a class of photovoltaic power systems," *IEEE Transactions on Power Apparatus and Systems*, vol. 102, pp. 3031-3037, Sept. 1983.